

PROCEEDINGS OF SPIE

SPIDigitalLibrary.org/conference-proceedings-of-spie

Design of freeform diffraction gratings: performance, limitations and potential applications

Ariadna Calcines, Cyril Bourgenot, Ray Sharples

Ariadna Calcines, Cyril Bourgenot, Ray Sharples, "Design of freeform diffraction gratings: performance, limitations and potential applications," Proc. SPIE 10706, Advances in Optical and Mechanical Technologies for Telescopes and Instrumentation III, 107064Z (10 July 2018); doi: 10.1117/12.2312125

SPIE.

Event: SPIE Astronomical Telescopes + Instrumentation, 2018, Austin, Texas, United States

Design of freeform diffraction gratings: performance, limitations and potential applications

Ariadna Calcines*^a, Cyril Bourgenot^a, Ray Sharples^a

^aDurham University, Centre for Advanced Instrumentation, DH1 3LE, United Kingdom.

ABSTRACT

Spectroscopy is a key technique in astronomy and nowadays most major telescopes include at least one spectrograph in their instrument suite. The dispersive element is one of the most important components and it defines the pupil size, spectral resolution and efficiency. Different types of dispersive elements have been developed including prisms, grisms, VPH and echelle gratings. In this paper, we investigate the design and optimization possibilities offered by metallic freeform gratings using diamond machining techniques. The incorporation of power in a diffraction grating enables several functionalities within the same optical component, such as the combination of dispersion, focusing and field reformat. The resulting benefit is a reduction in the number of surfaces and therefore, an improvement in the throughput. Freeform surfaces are also interesting for their enhanced optical performance by allowing extra degree of freedom in the optimization. These degrees of freedom include the shape of the substrate but also additional parameters such as the pitch or the number of blaze angle. Freeform gratings used as single optical component systems also present some limitations such as the trade-off between optical quality versus field of view or the spectral range versus spectral resolution. This paper discusses the possibility offered by the design of freeform gratings for low to medium spectral resolution, in the visible and near-infrared, for potential applications in ultra-compact integral field spectrographs.

Keywords: diffraction gratings, freeform gratings, freeform optics, Spectroscopy, Integral Field Spectroscopy, IFU, Image Slicers.

1. FREEFORM GRATINGS

The traditional spectrometer architecture is usually constituted of an achromatic collimator, a flat grating and an achromatic camera. Both, collimator and camera, are generally complex optical systems since they need to be achromatic over a large spectral range with minimal aberrations so the spatial and spectral resolutions remain optimal. Replacing these 3 elements with a single freeform surface offers a much simpler and compact solution but, as a result, bring inherent limitations. These limitations are discussed in this paper.

In this section, we investigate the design possibilities offered by metallic freeform gratings using diamond machining techniques, when used as a single element imaging spectrometer.

1.1 Definition of freeform gratings for optical design

There are different ways to define a freeform grating using Zemax Optic Studio. One of them is using “Elliptical Grating 1”, which combines an elliptical surface with polynomial aspheric terms and a grating, with the characteristic parameters associated to each. The grating can be modelled using standard parameters such as order, groove density and size.

*ariadna.calcines@durham.ac.uk; phone +44 191 334 4814.

Here the grating's freeform shape was considered to be an ellipse defined by three coefficients: the axes of the ellipse (a, b) and the radius of curvature (c). In this study, these parameters have been optimized using a merit function that minimizes the RMS spot radius measured at the image focal plane across the full field of view.

On top of the elliptical coefficients, some XY polynomial coefficients are also available for optimization, allowing the surface to deviate from the nominal elliptical shape. The grating's groove density (T) can also be optimized using additional parameters (α , β , Γ , Δ , ϵ). The reciprocal of the groove density (1/T), in units of micron per line, can be allowed to vary following a polynomial law described in Equation 1, adding an extra degree of freedom in the optimization. Y represents the grooves position across the surface.

$$\frac{1}{T} = d_{eff} = \frac{1}{T_0} + \alpha y + \beta y^2 + \Gamma y^3 + \Delta y^4 + \epsilon y^5 \quad (1)$$

1.2 Grating's initial specifications

The design of freeform gratings presents several variables. Thus, they can be designed and optimized for different specifications. In this study the grating was designed as a single element imaging system with the specifications presented in Table 1, inspired by the instrument IGIS¹, and with the idea of using this grating as a space borne hyperspectral imager.

The field of view is ± 0.57 degrees, corresponding to 11.94 Km swath, flying at an altitude of 600 km. This translates to an equivalent linear object size of ± 2 mm at the focus of a telescope with an effective focal length of 200 mm. A pupil diameter (grating size) of 10 mm was first considered with an output focal-ratio of F/9-10. The elliptical grating was designed to produce a magnification of 0.32, again as in the reference¹, and to work at first diffraction order. The magnification is defined as the ratio between the grating focal length and the distance between the object and the grating.

Working with a magnification smaller than 1 has the advantage of improving the instrument SNR, as well as allowing a substantial reduction of the detector size². For a specific detector size and number of grooves, gratings working at low diffraction order lead to a larger spectral coverage with good optical quality. On the other hand, gratings working at higher orders will offer a higher spectral resolution on a reduced spectral bandwidth. To spatially separate input and output beams, the ellipse is made off axis (40 mm)¹. Aiming for a spectral resolution of $R \approx 1,000$ and diffraction limited optical quality performance, the grating's period was calculated to be around 10 microns.

Table 1: Specifications considered for the initial freeform grating design.

Field of view	± 0.57 degrees $\equiv \pm 2$ mm object size
Output focal-ratio	F/9-10
Pupil diameter	10 mm
Magnification	0.32
Spectral resolution	$R \approx 1,000$
Off axis	40 mm
Spectral bandwidth	200 nm
Central wavelength	760 nm

1.3 Description of the grating's optimal shape for the initial specifications

The optimal surface shape obtained for the specifications of Table 1 working at conjugate points, evaluated at a wavelength of 760 nm with a spectral bandwidth of 200 nm, from 660 nm to 860 nm, is an ellipsoid tilted -11.1 degrees about the X axis.

A groove density of 150 lines/mm was initially considered, leading to a spectral resolution of $R=1,500$.

The grating is defined by the Zemax parameters presented in Table 2 and its layout is shown in Figure 1. For this grating, the input focal-ratio is $F/29.2$ and the output focal-ratio is $F/9.2$.

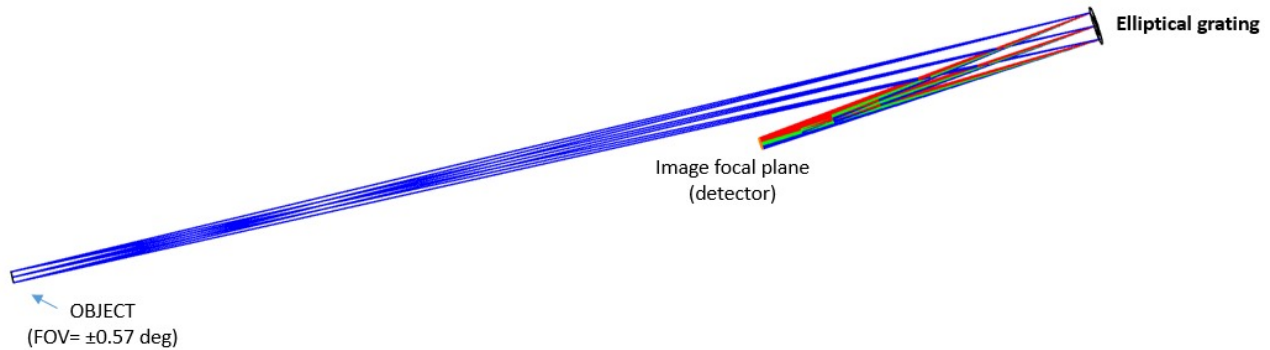


Figure 1. Optical design of the elliptical grating optimized for the specifications of Table 1.

The system presents diffraction limited optical quality for all defined field points, as shown in the spot diagram of Figure 2, evaluated for three wavelengths: 660 nm, 760 nm and 860 nm. The black circle is the Airy disc. Three different field points are defined for each wavelength associated to the central and extreme fields.

Table 2. Parameters associated to the elliptical grating optimized for order 1 for a spectral range from 660 nm to 860 nm and a groove density of 150 lines/mm.

Grating parameters	
a	0.003650
b	0.003635
c	-553.422
α	0.002939
β	0.0
Γ	0.0
Δ	0.0
ε	0.0

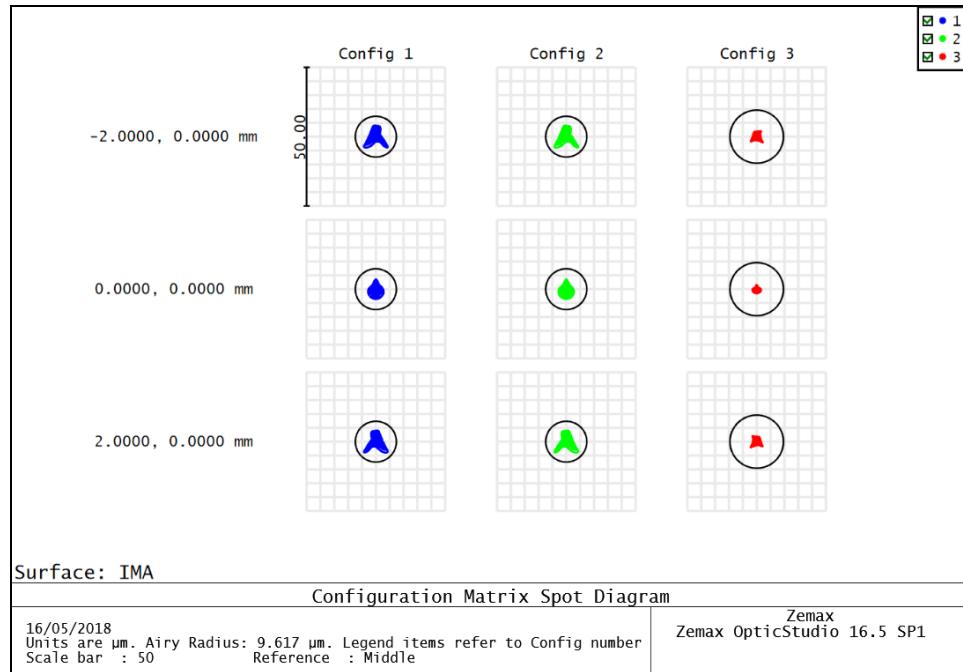


Figure 1: Diffraction limited spot diagram associated to the design of Figure 1 evaluated at the image focal plane at three wavelengths: 660 nm, 760 nm and 860 nm. At the detector position the size of the spectrum is 1.30 mm along the X axis and 2.70 mm along the Y axis.

The spectral bandwidth, initially set to 200 nm, was increased in order to establish the maximum spectral bandwidth that can be covered with this grating offering an optical quality at diffraction limit. The maximum spectral bandwidth was found to be $\Delta\lambda=540$ nm, which, in this case, corresponds to a linear size of 1.30 mm along the X axis by 7.26 mm along the Y axis. The optical quality is kept under the diffraction limit for a field of view of ± 3 mm along X and Y axes, equivalent to ± 0.61 degrees and can extend up to $\pm 3.5\text{mm}$ ($\pm 0.72^\circ$) with near diffraction limited optical performance.

2. INCREASING THE SPECTRAL RESOLUTION

The grating spectral resolution is a function of: (i) the order, (ii) the projection of the pupil diameter over the grating and (iii) the groove density. The variation of the spectral resolution with each of these parameters is evaluated in the following section.

2.1 Variation of the spectral resolution with the groove density

A groove density of 150 lines/mm was considered for the initial design (Figure 1), however, in order to increase the spectral resolution, the groove density was increased.

A minimum groove size of 4 μm was initially considered. In theory, it is possible to have sub-micron pitch, but the machining time and tool wear increase significantly, and thermal effects, even small, can become a limiting factor. As a result, 4 μm was set as a comfortable limit. Thus, the maximum groove density allowed, calculated as the inverse of the groove size, is 250 lines/mm. The spectral resolution, R , can be calculated applying Equation 2, where R is the spectral resolving power, N is the total number of illuminated grooves, m is the diffraction order, σ is the groove density and ϕ_{pup} is the pupil diameter. In our case, since the grating is placed at the pupil position, this is also the grating diameter.

$$R = N \cdot m = \sigma \cdot \phi_{\text{pup}} \cdot m \quad (2)$$

For a pupil size of 10 mm and working at first diffraction order, the optimal spectral resolution for a groove density of 150 lines/mm is $R=1,500$, while when increasing the groove density to 250 lines/mm the spectral resolution is 2,500. The grating layout was evaluated using 250 lines/mm obtaining equivalent optical performance. In this case the input focal-ratio is $F/28.1$ and the output focal-ratio is $F/9.2$. The magnification of the system is 0.33.

2.2 Variation of the spectral resolution with the pupil diameter

As indicated in Equation 2, the spectral resolution is also a function of the pupil diameter. Figure 3 shows the linear dependence of the spectral resolution with the pupil diameter. With a groove density set at 250 lines/mm, and for pupil sizes ranging from 1 mm to 25 mm, the spectral resolution varies from 250 to 6,250 at diffraction order 1.

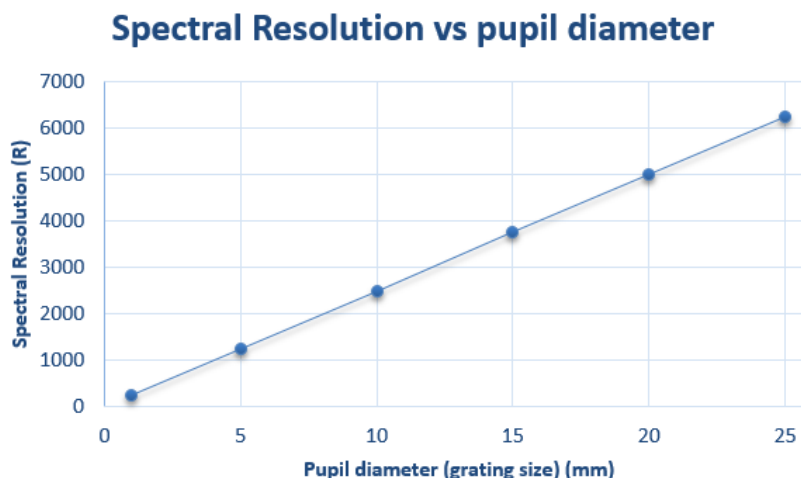


Figure 3. Linear dependence of the spectral resolution with the pupil diameter. For pupil sizes from 1 mm to 25 mm, the value of the spectral resolution varies from 250 to a resolution of 6,250.

A grating with a diameter of 25 mm was optimized for diffraction limited optical quality. The grating parameters obtained from the optimization are shown in Table 3. In this case, the entrance focal-ratio is $F/15.9$ and the output focal-ratio is $F/14$, equivalent to a system magnification of 0.88.

Table 1: Grating values obtained for the design optimized for a pupil diameter of 25 mm.

Grating parameters	
a	0.002672
b	0.002682
c	-376.587
α	-0.001865
β	0.0
Γ	0.0
Δ	0.0
ε	0.0

2.3 Variation of the spectral resolution with the diffraction order

The spectral resolution depends also on the diffraction order as shown in Figure 4. For orders between 1 and 9, the value of the spectral resolution varies from 6,250 to 56,250. These results have been calculated considering a groove density of 250 lines/mm and a pupil diameter of 25 mm. The optimization at different orders allows the improvement of the spectral resolution and the potential application for a wider range of science cases.



Figure 4. Linear dependence of the spectral resolution with the diffraction order for a groove density of 250 lines/mm and a pupil diameter of 25 mm.

In Figure 5, a pupil size of 25 mm was considered, with a groove density of 250 lines/mm and three wavelengths: 740 nm, 760 nm and 780 nm. For each diffraction order tested, the grating parameters were re-optimized to improve the optical quality. Thus, each case corresponds to different grating parameters.

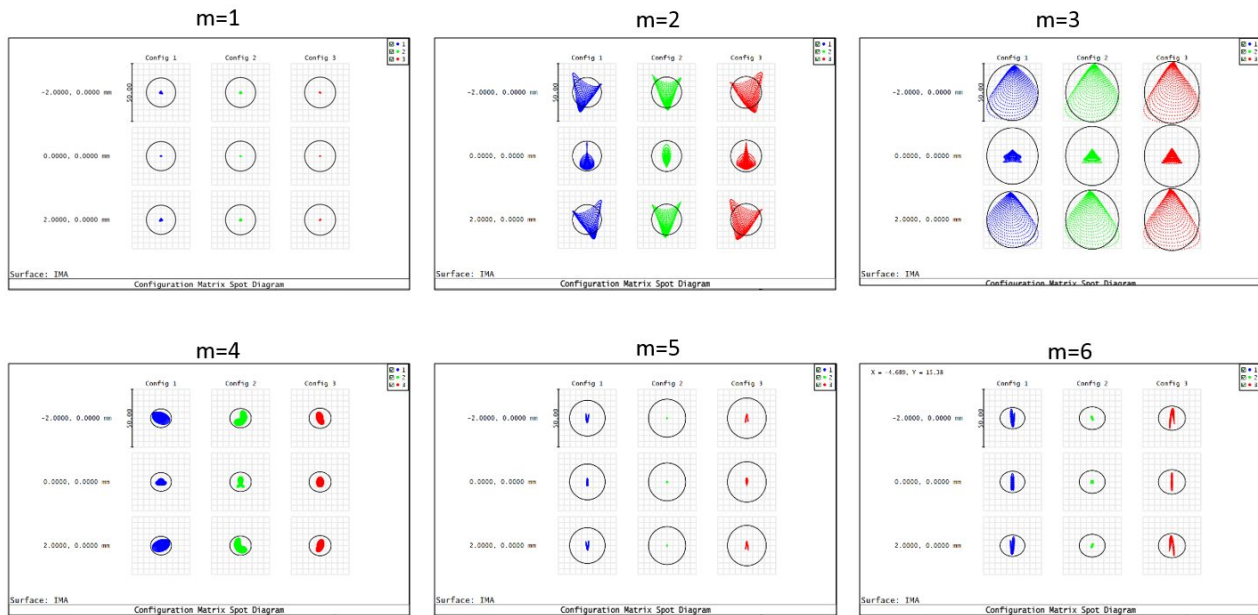


Figure 5. Optical quality obtained for different diffraction orders (m) for a spectral range from 740 nm to 780 nm. A pupil size of 25 mm and a groove density of 250 lines/mm are considered in all cases. Each design considers different grating parameters.

The design parameters of the gratings can be optimized for larger diffraction orders obtaining thus a larger spectral resolution, however, the increment in the order implies a reduction in the spectral bandwidth, which would be, in some cases, a clear limitation for potential applications.

3. EFFECT OF VARIABLY SPACED GROOVES

Ideally, a grating has its grooves equally and constantly spaced on the surface as seen from a perspective normal to the surface. Consequently, from a machining point of view, a constant period on a curved surface does not translate into a constant increment along the machine axis, as it would be for a flat grating, but leads to a variable machine's increment. The compensation of this effect while ruling the grating adds a layer of complexity in the tool path calculation and can be neglected (by keeping the increment constant) in most of the cases if the curvature remains small. In this study, we estimate the gain in optical quality over the spectral direction if the machine's increment is made variable.

If the pitch is made linearly variable, the spatial and spectral resolutions can be improved further. The optimization is done on the coefficient α in the Equation 3 (using Zemax nomenclature):

$$1/T = (1/T_0) + \alpha \cdot x \quad (3)$$

Where T is the effective period (in micron) at position x ; T_0 is the nominal period; α is the coefficient in units of line per micron and x is the aperture coordinate in mm. At the center of the grating where $x = 0$, a 10 microns pitch was considered. For $x \neq 0$, the curvature of the grating introduces a variation in the distance between each groove as shown in Figure 6.

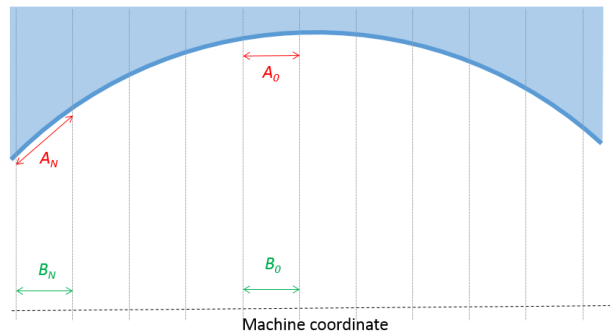


Figure 6. Effective groove space variation on a high gradient freeform surface. B_0 is the machine increment at the center of the aperture. When a constant increment $B_N = B_0$ is projected onto the surface at the edge of the aperture, the effective period A becomes larger than the increment.

This effect is more important when the curvature is larger, with higher order gratings and with larger off axis distance.

4. DESIGN OF DUAL BLAZED GRATING

An interesting advantage offered by 5 axes diamond machining is the control of the blaze angle on a curved surface. Multi-blaze can also be considered.

Echelette gratings present a pattern of lines with the same inclination (blaze angle) designed to obtain the maximum efficiency in a specific diffraction order and for a wavelength called blaze wavelength. It is also possible to have more than one blaze angle (multi-blaze) to maximize the grating efficiency at different wavelengths. A dual blaze structure is shown in Figure 7.

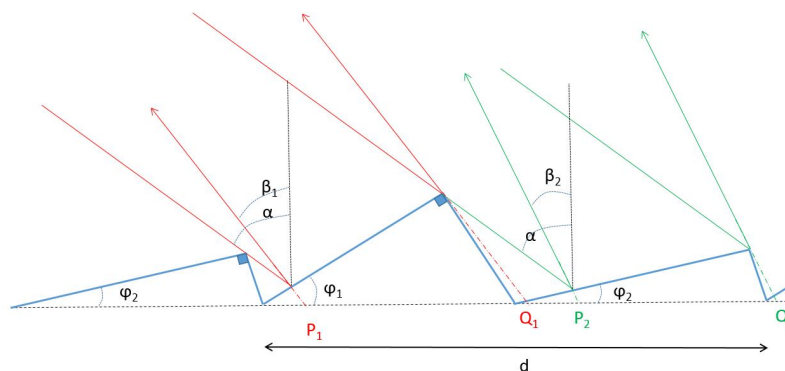


Figure 7. Multi blazed grating and geometric construction for the derivation of the grating efficiency formula.

In the reference³, Equation 5, the overall phase difference in the diffracted wave for a wavelength λ induced by a groove in a single blaze configuration is:

$$\theta(\phi) = \frac{2\pi}{\lambda} PQ [\sin(\alpha - \beta) + \sin(\beta - \phi)] \quad (4)$$

Where PQ is the segment illuminated by the incident light. The diffracted beam is given by the Fourier's transform of the window function $a(x)$, where:

$$a(x) = U_a \cdot e^{i\theta(\phi)} \quad (5)$$

U_a is the unit box of width a .

For 2 blaze angles:

$$a(x) = a_1(x) + a_2(x) \quad (6)$$

And

$$A(\sigma) = A_1(\sigma) + A_2(\sigma) \quad (7)$$

Where a_1 and a_2 are the window functions for the blaze 1 and blaze 2 respectively, and each window function has a phase $\theta_1(\phi_1)$ and $\theta_2(\phi_2)$. $A(\sigma)$ denotes the diffracted beam, and it is given by the Fourier's transform of the window function $a(x)$.

The amplitude of the diffracted beam for a single blaze case is described by the Equation 17 in the same reference paper³. In our analysis, it is possible to include simultaneously the contributions of the blaze 1 and blaze 2 in Equation 7, as described in Equation 8:

$$A = e^{i\Delta\theta(0)} \cdot \left(\text{sinc}\left(\frac{\theta_1(\phi_1)}{2}\right) + \text{sinc}\left(\frac{\theta_2(\phi_2)}{2}\right) \right) \quad (8)$$

The phase contribution of each blaze structure is a function of PQ, which, in each case, can be described as follows:

$$P_1Q_1 = \frac{d}{2 \cdot \cos \phi_1} - \frac{d \cdot \sin \phi_2 \cdot \tan(\alpha - \phi_1)}{2 \cdot \cos(\phi_1 - \phi_2)} \quad (9)$$

$$P_2Q_2 = \frac{d}{2 \cdot \cos \phi_2} - \frac{d \cdot \sin \phi_1 \cdot \tan(\alpha - \phi_2)}{2 \cdot \cos(\phi_1 - \phi_2)} \quad (10)$$

The intensity of the diffracted wave is then described by the Equation 11:

$$I = \frac{1}{4} \text{sinc}^2\left(\frac{\theta_1(\phi_1)}{2}\right) + \frac{1}{4} \text{sinc}^2\left(\frac{\theta_2(\phi_2)}{2}\right) + \frac{1}{2} \text{sinc}\left(\frac{\theta_1(\phi_1)}{2}\right) \cdot \text{sinc}\left(\frac{\theta_2(\phi_2)}{2}\right) \quad (11)$$

The normalization factor is calculated for the condition $\phi_1 = \phi_2$.

The efficiency of a dual blazed grating was compared with that of a single blazed grating, as shown in Figure 8. The single blaze grating has a blaze angle of 1.68 degrees and it was optimized at 580 nm blaze wavelength, as it is clearly presented by the maximum of its efficiency curve (in green). The blaze angles for the multi-blaze grating are 1.35 degrees and 3 degrees. In blazed gratings, most of the power is concentrated in a particular order and associated to a wavelength of maximum efficiency, the blaze wavelength. For multi-blaze, the efficiency curve will present as many peak wavelengths as the number of blaze angles, two in this case. According to our model, a dual blaze structure can be interesting in configurations where a broader efficiency (relative efficiency between different wavelengths) is required, or when there is more than one priority wavelength. This can be achieved at the cost of the absolute efficiency (maximum intensity diffracted).

The combined effect of 2 different blaze angles induces a drop in the total efficiency of about 20% when comparing the dual blaze freeform grating and that associated to single blaze.

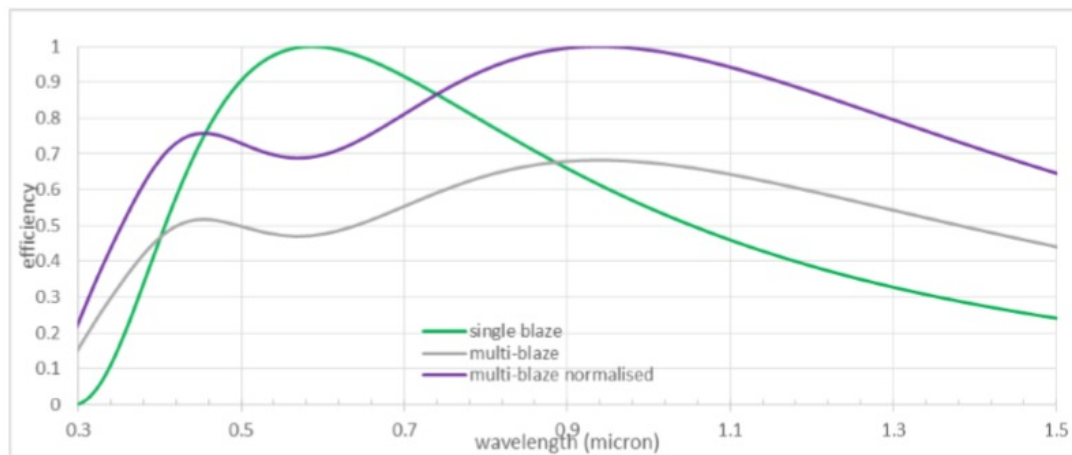


Figure 8. Single and dual blaze structure comparison. Single blaze is at 1.68° and dual blaze is at 1.35° and 3°. The efficiency curve in multi-blaze configuration will present as many peak wavelengths as the number of different blaze angles.

5. APPLICATION FOR ULTRA-COMPACT INTEGRAL FIELD SPECTROGRAPHS

The advantages of Integral Field Spectrographs⁴ (IFS) in Astronomy have led to significant developments in different components such as: Integral Field Units (IFUs), dispersive elements or detectors. In the search for instrumentation with higher resolution, observing larger fields of view with better signal-to-noise, the developments usually pay the cost of: much larger and heavier instruments, a reduction of the throughput, stability, thermal effects and increments in budget and leading time. These are not exclusive problems of Astronomy, equivalent problems are found in Earth Observation or other science applications.

In the last few decades, the desire for refined models of climate change has motivated the need for even more reliable and precise Earth Observation (EO) data. This has been a key driver in the development of hyperspectral instrumentation, and one of the challenges that faces future EO instruments is to accommodate a larger spectral range with better spatial and spectral resolution. A second challenge is the improvement of temporal sampling, which drives the technology towards smaller satellite platforms and ultra-compact payloads.

IFS⁴ are composed by an IFU that reorganizes a bidimensional field of view into one or more slits to feed a spectrograph, plus the components of the spectrograph itself (collimator, dispersive element, camera and detector). This study investigates a specific set-up that combines the elements of an Image Slicer⁶ based IFU with those of the spectrograph. This idea was originally presented and developed by the University of Florida¹. Durham University participated in the manufacturing and, due to the potential of these systems for many different applications, we decided to continue investigating this solution for ultra-compact Integral Field Spectrographs proposals.

An Image Slicer is composed by different arrays of mirrors: slicer mirrors to slice the field of view; pupil mirror (or pupil mask) to control the intermediate pupil image and slit or field mirrors to focus the beams generating the output slit or slits. The key of this proposal is the use of powered slicer mirrors that generate a pupil image at their focal length and freeform blazed gratings at that pupil position. An array of freeform gratings is then required, with a grating per slicer mirror, as shown in the example of Figure 9.

The freeform grating achieves three optical functions at the same time:

- Spectral dispersion
- Re-imaging: since the gratings have curvature they will generate an image (spectrum) at their focal length. They also offer control of the magnification through the grating focal length.
- Reformatting: the tilt angle about the three axes (X, Y, Z) allows each single grating to reorganize the spectrum associated to each slice of the field of view aligned adequately to compose the total spectrum. It also allows the control of the output angles for telecentric systems.

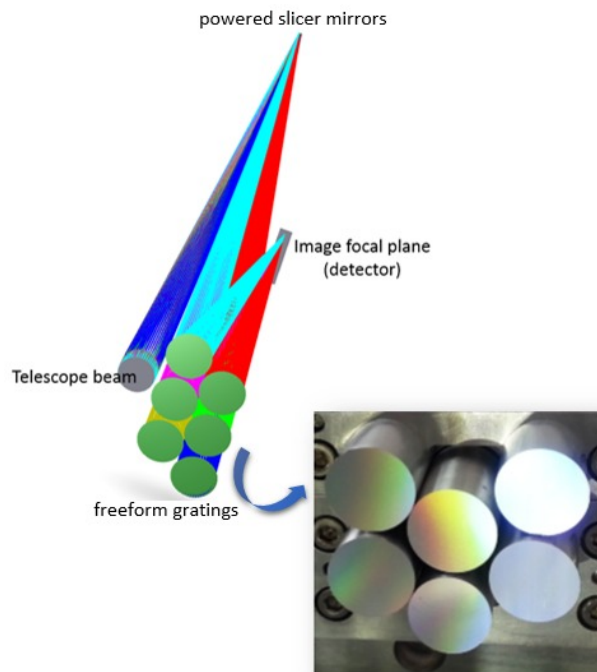


Figure 9. On the left: example of the layout of an ultra-compact Integral Field Spectrograph combining powered slicer mirrors at the telescope image focal plane and freeform gratings at the pupil position. Each grating generates the spectrum associated to a slice of the field of view onto the detector. On the right: an array of freeform gratings¹ manufactured at Durham University.

This highly modular concept opens a new window on the design of future compact and modular spectral imagers. The ultra-compactness of the design, combined with the financially competitive manufacturing process, will make multi-channel imaging spectrographs ideal candidates for deployment on small Earth Observation satellites similar to Proba-V and possibly in future CubeSat missions. Similar designs can also be considered for use on airborne platforms and at ground level with low and medium spectral resolution.

6. CONCLUSIONS

The goal of this study is to investigate different design alternatives of freeform gratings, optimization of their performance, identify their limitations and present some of their potential applications.

The use of freeform gratings simplifies the optics required for Integral Field Spectrographs, leading to ultra-compact solutions that reduce the price and weight of the payload. These solutions combine the optical components of an Image Slicer based Integral Field Unit with those of the spectrograph, offering compact systems with only two optical components.

Diamond machining techniques can offer a cost effective solution for low to mid spectral resolution instrumentation. In addition, all components could be manufactured of the same material avoiding thermal variations.

The gratings can be designed and manufactured for custom sets of specifications avoiding the limitations of commercial components. Some of the flexible parameters are: size, groove density, blaze wavelength, efficiency, blaze angle, resolution, focal-ratio, magnification (focal length) and spectral range.

There also exist some limitations when freeform gratings are used as a single component imaging system:

- These gratings are recommended for low and medium spectral resolution ($R \leq 15,000$).
- Low diffraction orders ($m=1$ or 2) are compatible with a bandwidth in the range of 20% to 70% the central wavelength in order to keep the optical quality below the diffraction limit.
- Higher diffraction orders ($m > 6$) will have a restricted bandwidth in the range of 1% to 5% of the central wavelength in order to keep the optical quality under the diffraction limit.

It is possible to design and manufacture gratings with more than one blaze angle (multi-blaze) and with variable spacing to improve the spectral resolution for highly curved surfaces.

7. ACKNOWLEDGMENT

This work has been developed in the framework of a CEOI (Centre of Earth Observation Instrumentation) pathfinder grant.

REFERENCES

- [1] Bourgenot, C.; Robertson, D. J.; Stelter, D.; Eikenberry, S., “Towards freeform Freeform blazed gratings using diamond machining,” SPIE Proc. 9912, 99123M (2016).
- [2] De Clercq, C., et al., “ELOIS: an innovative spectrometer design using a freeform grating”, Opt. Syst. Des. 2015 Opt. Des. Eng. VI, vol. 9626 (2015).
- [3] Casini, R.; Nelson, P. G., “On the intensity distribution function of blazed reflective diffraction gratings,” J Opt Soc Am A Opt Image Sci Vis, vol. 31, no. 10, pp. 2179–2184 (2014).
- [4] Chou, Richard C. Y.; Moon, Dae-Sik; Eikenberry, Stephen S., “The optical design of wide integral field infrared spectrograph”, SPIE Proc. 7735, 77356S (2010).
- [5] Calcines, A.; Lopez, R.L.; Collados, M., “MuSICa: the multi-slit image slicer for the EST spectrograph”, Journal of Astronomical Instrumentation, Vol. 02, 1350009 (2013).